

Overview — "Active Contours Without Edges"

By Tony F. Chan, and Luminita A. Vese

Presented by: Camilo Martínez

Universität des Saarlandes

June, 2024



UNIVERSITÄT
DES
SAARLANDES

① Motivation

② The Chan–Vese Model

③ Results

④ Impact on Research

⑤ Concluding Remarks

⑥ References

① Motivation

A (brief) Introduction to Image Segmentation

Predecessors to the Chan-Vese Model

② The Chan–Vese Model

③ Results

④ Impact on Research

⑤ Concluding Remarks

⑥ References

① Motivation

A (brief) Introduction to Image Segmentation

Predecessors to the Chan-Vese Model

② The Chan–Vese Model

③ Results

④ Impact on Research

⑤ Concluding Remarks

⑥ References

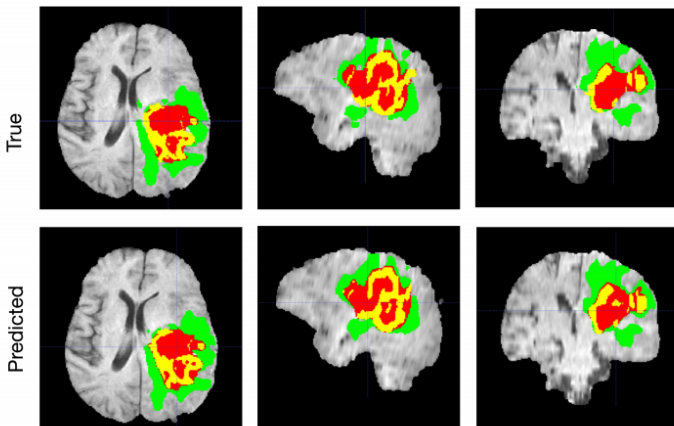
A (brief) Introduction to Image Segmentation

- One of the most widely studied problems in *Computer Vision*.
 - Applicable in **medical imaging, robotics, video surveillance, materials science, autonomous driving**, and many others.



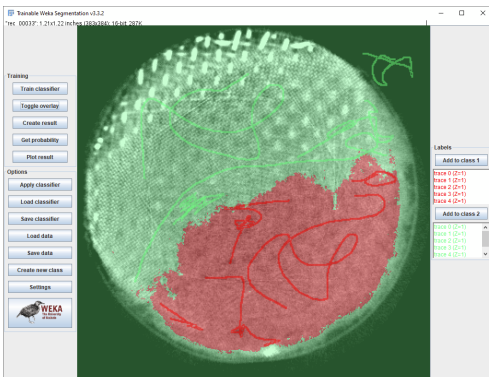
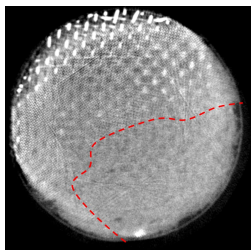
Image segmentation in autonomous driving [21] (2024)

A (brief) Introduction to Image Segmentation



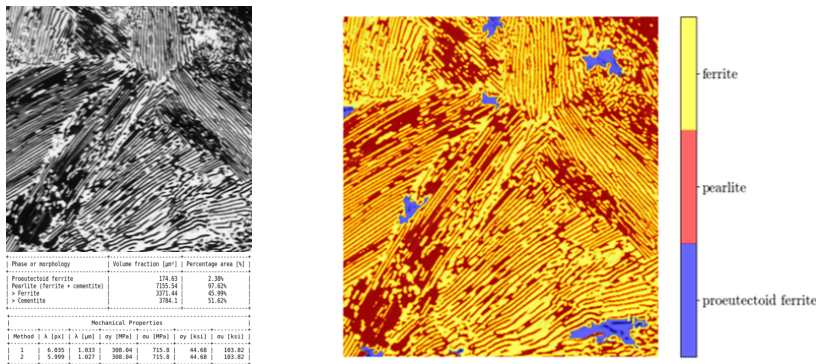
A typical segmentation example for *tumor segmentation*. The predicted segmentation results match the ground truth well [22] (2018).

A (brief) Introduction to Image Segmentation



Slice of micro-CT of a solid cylindrical sample covered with a two metallic nets: inner is fine and outer is coarse. Segmentation done in **ImageJ**'s Trainable Weka Segmentation plugin [23] (2022).

A (brief) Introduction to Image Segmentation



Low-carbon steel microstructure, segmented into **ferrite** and **pearlite** phases. The segmentation results are used to calculate the mechanical properties of the material [16] (2021).

① Motivation

A (brief) Introduction to Image Segmentation

Predecessors to the Chan–Vese Model

② The Chan–Vese Model

③ Results

④ Impact on Research

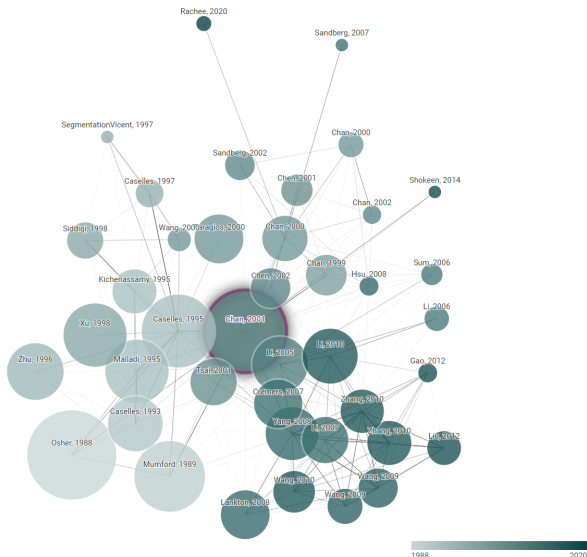
⑤ Concluding Remarks

⑥ References

Predecessors to the Chan-Vese Model

- **Early methods:** thresholding, region growing, edge-based segmentation.
- **Improvements:** snakes and active contours models.
- Challenges *so far*: segmentation without clear edges.

| Title | Authors | Year |
|--|------------------------|------|
| Boundary detection by minimizing functionals [9] | D. Mumford and J. Shah | 1985 |
| Snakes: Active contour models [7] | M. Kass et al. | 1988 |
| A topology independent shape modeling scheme [6] | R. Malladi et al. | 1993 |
| On geodesic active contours [2] | V. Caselles et al. | 1997 |



Prior and Derivative Works of the Chan-Vese Model. Courtesy of @ConnectedPapers,
this graph available [here](#).



① Motivation

② The Chan–Vese Model

The "Fitting" Problem

The Level-Set Formulation

Energy Minimization & Discretization

③ Results

④ Impact on Research

⑤ Concluding Remarks

⑥ References

① Motivation

② The Chan–Vese Model

The "Fitting" Problem

The Level-Set Formulation

Energy Minimization & Discretization

③ Results

④ Impact on Research

⑤ Concluding Remarks

⑥ References

The "Fitting" Problem

- **Chan and Vese (2001)** proposed a specific region-based active contour model, where the image is segmented into **two phases/regions**: object and background.
- Assume we have an image $u(x), x \in \Omega$, and the image is formed by two regions with mean intensity values: u_{in} and u_{out} .
- Our *evolving* boundary curve C separates the two regions.
- Then, we can define a *fitting* term that penalizes deviations from the mean intensity values:

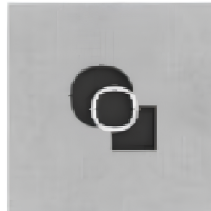
$$\text{fitting}(C) := F_{in}(C) + F_{out}(C)$$

The "Fitting" Problem

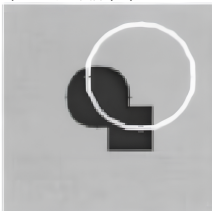
$$F_{in}(C) > 0, F_{out}(C) \approx 0, \text{fitting} > 0$$



$F_{in}(C) \approx 0$, $F_{out}(C) > 0$, fitting > 0



$F_{in}(C) > 0$, $F_{out}(C) > 0$, fitting > 0



$$F_{in}(C) \approx 0, F_{out}(C) \approx 0, \text{fitting} = 0$$



Consider all possible cases of C enclosing the object in the image. The *fitting* term is minimized only in the case when C is exactly on the boundary of the object [1].

The "Fitting" Problem

- Furthermore, using a Mean-Squared Error (MSE) approach,

$$\begin{aligned} \text{fitting}(C) &= F_{in}(C) + F_{out}(C) \\ &= \underbrace{\int_{\text{inside}(C)} |u(\mathbf{x}) - c_{in}|^2 d\mathbf{x}}_{> 0, \text{ if } u(\mathbf{x}) \text{ deviates from } c_{in}} + \underbrace{\int_{\text{outside}(C)} |u(\mathbf{x}) - c_{out}|^2 d\mathbf{x}}_{> 0, \text{ if } u(\mathbf{x}) \text{ deviates from } c_{out}} \end{aligned}$$

- Thus, our minimizer C_0 that satisfies $\text{fitting}(C_0) \approx 0$ can be defined as:

$$C_0 = \inf_C \{\text{fitting}(C)\} = \inf_C \{F_{in}(C) + F_{out}(C)\}$$

Formulation as an Energy Functional

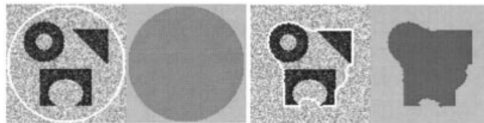
- We can introduce the energy functional $F(c_{in}, c_{out}, C)$ as:

$$F(c_{in}, c_{out}, C) = \underbrace{\mu \cdot \text{Length}(C) + \nu \cdot \text{Area}(\text{inside}(C))}_{\text{penalize the "size" of } C} + \text{fitting}(C)$$

where $\mu, \nu \in \mathbb{R}_0^+$.

- Thus, the minimization problem becomes:

$$C_0 = \inf_{c_{in}, c_{out}, C} F(c_{in}, c_{out}, C).$$



Shrinking contour C , detecting different objects from a noisy image with various shapes.

Left: u and the contour. **Right:** the piecewise-constant approximation of u [1].

Formulation as an Energy Functional

- Finally,

$$\begin{aligned} F(c_{in}, c_{out}, C) = & \mu \cdot \text{Length}(C) + \nu \cdot \text{Area}(\text{inside}(C)) \\ & + \lambda_1 \int_{\text{inside}(C)} |u(\mathbf{x}) - c_{in}|^2 d\mathbf{x} \\ & + \lambda_2 \int_{\text{outside}(C)} |u(\mathbf{x}) - c_{out}|^2 d\mathbf{x} \end{aligned}$$

where $\mu, \nu \in \mathbb{R}_0^+$, $\lambda_1, \lambda_2 \in \mathbb{R}^+$ are fixed parameters.

- Usually $\lambda_1 = \lambda_2 = 1$ and $\nu = 0$.
- This can be formulated and solved using the **level set method** [8].

Comparison with the Mumford–Shah Model

- The **Mumford–Shah model** is defined as [17]:

$$E_{MS}(K, u) = \int_{\Omega} (f - u)^2 dx + \gamma \int_{\Omega \setminus K} |\nabla u|^2 dx + \lambda |K|$$

- The **Mumford–Shah model** leads to the **Chan–Vese** approach

- if we have piecewise constant approximations u , i.e.,
 $u = \text{constant } c_i$ on each connected component R_i of $\Omega \setminus C$.
- and an edge set K that separates Ω into two phases.

- This reduced case is called the *minimal partition problem* [1].

① Motivation

② The Chan–Vese Model

The "Fitting" Problem

The Level-Set Formulation

Energy Minimization & Discretization

③ Results

④ Impact on Research

⑤ Concluding Remarks

⑥ References

The Level-Set Formulation

- In the **level set method** [8], $C \subset \Omega$ is represented by the zero level set of a **Lipschitz function** $\phi : \Omega \rightarrow \mathbb{R}$, such that

$$\begin{cases} C = \partial\omega = \{(x, y) \in \Omega : \phi(x, y) = 0\}, \\ \text{inside}(C) = \omega = \{(x, y) \in \Omega : \phi(x, y) > 0\}, \\ \text{outside}(C) = \Omega \setminus \bar{\omega} = \{(x, y) \in \Omega : \phi(x, y) < 0\}. \end{cases}$$

Recall that...

A function $f : \mathbb{R} \rightarrow \mathbb{R}$ is called a **Lipschitz function** if $\exists L \geq 0$ such that $\forall x_1, x_2 \in \mathbb{R}$,

$$|f(x_1) - f(x_2)| \leq L|x_1 - x_2|.$$

Intuitively, a **Lipschitz function** is limited in how fast it can change: there exists a real number such that, for every pair of points on the graph of this function, the absolute value of the slope of the line connecting them is not greater than this real number; the smallest such bound is called the **Lipschitz constant** of the function, L [18].

The Level-Set Formulation

- Our aim is to compute the *Euler-Lagrange* equation associated with the introduced energy functional $F(c_{in}, c_{out}, C)$.
- Thus, we replace the unknown variable C by the unknown variable ϕ [10].

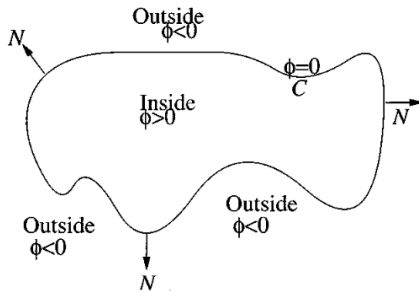
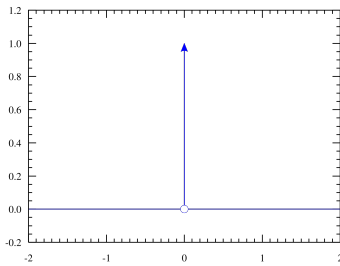
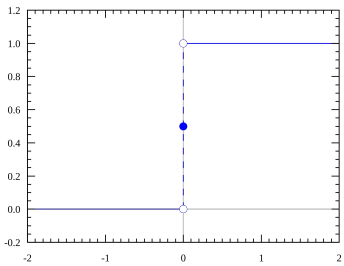


Illustration for the relationship between C and ϕ ; Curve $C = \{(x, y) : \phi(x, y) = 0\}$ propagating in normal direction [1].

The Level-Set Formulation

- On the other hand, we can define the *Heaviside* function $H(z)$ and the *Dirac delta* function $\delta_0(z)$ as:

$$H(z) = \begin{cases} 0, & \text{if } z < 0 \\ 1, & \text{if } z \geq 0 \end{cases}, \quad \delta_0(z) = \frac{d}{dz} H(z) = \begin{cases} \infty, & \text{if } z = 0, \\ 0, & \text{if } z \neq 0. \end{cases}$$



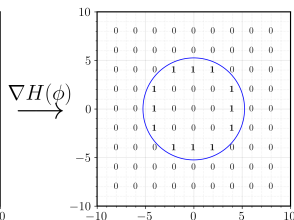
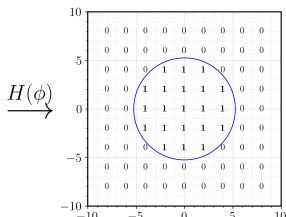
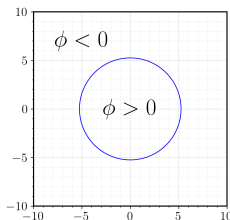
Left: Heaviside function $H(z)$ [19], **Right:** its derivative $\delta_0(z)$, the one-dimensional Dirac measure [20].

The Level-Set Formulation

- With these definitions, it's clear that:

$$\text{Length}\{\phi = 0\} = \int_{\Omega} |\nabla H(\phi(\mathbf{x}))| d\mathbf{x} = \int_{\Omega} \delta_0(\phi(\mathbf{x})) |\nabla \phi(\mathbf{x})| d\mathbf{x},$$

$$\text{Area}\{\phi \geq 0\} = \int_{\Omega} H(\phi(\mathbf{x})) d\mathbf{x}$$



From left to right, the process of applying H to ϕ and then taking the gradient.

The Level-Set Formulation

- Thus, our energy functional $F(c_{in}, c_{out}, \phi)$ can be rewritten as:

$$\begin{aligned}
 F(c_{in}, c_{out}, \phi) &= \underbrace{\mu \int_{\Omega} \delta(\phi(\mathbf{x})) |\nabla \phi(\mathbf{x})| d\mathbf{x}}_{\text{Length(C)}} + \nu \underbrace{\int_{\Omega} H(\phi(\mathbf{x})) d\mathbf{x}}_{\text{Area(inside(C))}} \\
 &\quad + \lambda_1 \underbrace{\int_{\Omega} |u(\mathbf{x}) - c_{in}|^2 H(\phi(\mathbf{x})) d\mathbf{x}}_{= \int_{inside(C)} |u(\mathbf{x}) - c_{in}|^2 d\mathbf{x}} \\
 &\quad + \lambda_2 \underbrace{\int_{\Omega} |u(\mathbf{x}) - c_{out}|^2 (1 - H(\phi(\mathbf{x}))) d\mathbf{x}}_{= \int_{outside(C)} |u(\mathbf{x}) - c_{out}|^2 d\mathbf{x}}
 \end{aligned}$$

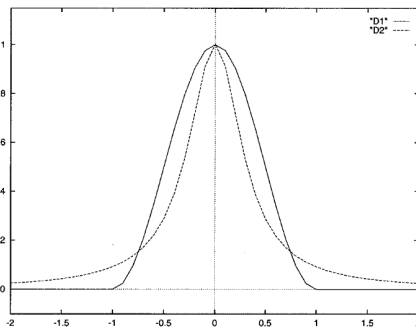
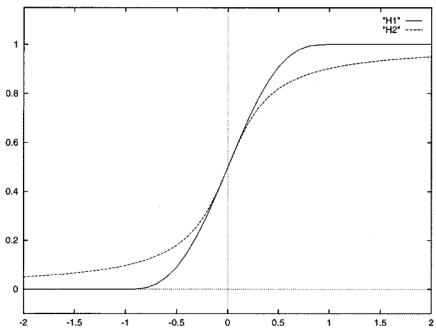
The Level-Set Formulation

- In practice, H and δ_0 are approximated by *continuous functions* H_ϵ and δ_ϵ , respectively, such that H_ϵ is at least $C^2(\bar{\Omega})$ and $\lim_{\epsilon \rightarrow 0} H_\epsilon(z) = H(z)$ and $\lim_{\epsilon \rightarrow 0} \delta_\epsilon(z) = \delta_0(z)$.
- **Chan and Vese (2001)** tried a $C^2(\bar{\Omega})$ regularization $H_{1,\epsilon}$, proposed in [10] and introduced a $C^\infty(\bar{\Omega})$ regularization $H_{2,\epsilon}$, defined as:

$$H_{1,\epsilon}(z) = \begin{cases} 1 & \text{if } z > \epsilon \\ 0 & \text{if } z < -\epsilon \\ \frac{1}{2} \left[1 + \frac{z}{\epsilon} + \frac{1}{\pi} \sin\left(\frac{\pi z}{\epsilon}\right) \right] & \text{if } |z| \leq \epsilon \end{cases}$$

$$H_{2,\epsilon}(z) = \frac{1}{2} \left(1 + \frac{2}{\pi} \arctan\left(\frac{z}{\epsilon}\right) \right)$$

The Level-Set Formulation



Two different regularizations of the (left) heaviside function H and (right) delta function δ_0 [1].

The Level-Set Formulation

- Finally, our *regularized* energy functional $F_\epsilon(c_{in}, c_{out}, \phi)$ is given by:

$$\begin{aligned} F(c_{in}, c_{out}, \phi) = & \mu \int_{\Omega} \delta_\epsilon(\phi(\mathbf{x})) |\nabla \phi(\mathbf{x})| d\mathbf{x} + \nu \int_{\Omega} H_\epsilon(\phi(\mathbf{x})) d\mathbf{x} \\ & + \lambda_1 \int_{\Omega} |u(\mathbf{x}) - c_{in}|^2 H_\epsilon(\phi(\mathbf{x})) d\mathbf{x} \\ & + \lambda_2 \int_{\Omega} |u(\mathbf{x}) - c_{out}|^2 (1 - H_\epsilon(\phi(\mathbf{x}))) d\mathbf{x} \end{aligned}$$

① Motivation

② The Chan–Vese Model

The "Fitting" Problem

The Level-Set Formulation

Energy Minimization & Discretization

③ Results

④ Impact on Research

⑤ Concluding Remarks

⑥ References

Euler-Lagrange Equation

- Keeping c_{in} and c_{out} fixed, and minimizing F_ϵ with respect to ϕ , we deduce the associated **Euler–Lagrange** equation for ϕ :

$$\begin{cases} F_\phi = \nu\delta_\epsilon(\phi) + \lambda_1|u - c_{in}|^2\delta_\epsilon(\phi) - \lambda_2|u - c_{out}|^2\delta_\epsilon(\phi), \\ F_{\phi_x} = 2\mu\delta_\epsilon(\phi)\phi_x, \\ F_{\phi_y} = 2\mu\delta_\epsilon(\phi)\phi_y \end{cases}$$

Recall that...

The **Euler–Lagrange equation** for an energy functional of the form $E(\phi) = \int_\Omega F(x, y, \phi, \phi_x, \phi_y) dx$ is $F_\phi - \partial_x F_{\phi_x} - \partial_y F_{\phi_y} = 0$ with *natural boundary conditions* $\mathbf{n}^\top \begin{pmatrix} F_{\phi_x} \\ F_{\phi_y} \end{pmatrix} = 0$ where \mathbf{n} denotes a normal vector to the image boundary $\partial\Omega$.

Euler-Lagrange Equation

- Thus, for $t \geq 0$, we get:

$$\begin{aligned}\frac{\partial\phi}{\partial t} &= \delta_\epsilon(\phi) \left[\mu \operatorname{div} \left(\frac{\nabla\phi}{|\nabla\phi|} \right) - \nu - \lambda_1(u - c_{in})^2 + \lambda_2(u - c_{out})^2 \right] \\ &= 0 \quad \text{in } (0, \infty) \times \Omega\end{aligned}$$

- With initial contour $\phi(0, x, y) = \phi_0(x, y)$ in Ω and boundary condition:

$$\frac{\delta_\epsilon(\phi)}{|\nabla\phi|} \frac{\partial\phi}{\partial\vec{n}} = 0 \quad \text{on } \partial\Omega$$

where \vec{n} denotes the exterior normal to the boundary $\partial\Omega$, and $\partial\phi/\partial\vec{n}$ denotes the normal derivative of ϕ at the boundary.

Discretization

- To discretize this equation in ϕ , **Chan and Vese(2001)** used a *finite differences implicit scheme*.

Usual Notations in Finite Differences

- Let h be **space step**; Δt , **time step**, and $(x_i, y_j) = (ih, jh)$ be the grid points, for $1 \leq i, j \leq M$.
- Let $\phi_{i,j}^n = \phi(n\Delta t, x_i, y_j) \approx \phi(t, x, y)$, with $n \geq 0$, $\phi^0 = \phi_0$.
- The finite differences are:

$$\Delta_-^x \phi_{i,j} = \phi_{i,j} - \phi_{i-1,j}, \quad \Delta_+^x \phi_{i,j} = \phi_{i+1,j} - \phi_{i,j},$$

$$\Delta_-^y \phi_{i,j} = \phi_{i,j} - \phi_{i,j-1}, \quad \Delta_+^y \phi_{i,j} = \phi_{i,j+1} - \phi_{i,j}$$

Discretization

- The following discretization and linearization of the PDE is used by **Chan and Vese (2001)**:

$$\begin{aligned} \frac{\phi_{i,j}^{n+1} - \phi_{i,j}^n}{\Delta t} = & \delta_h(\phi_{i,j}^n) \left[\frac{\mu}{h^2} \Delta_-^x \right. \\ & \cdot \left(\frac{\Delta_+^x \phi_{i,j}^{n+1}}{\sqrt{(\Delta_+^x \phi_{i,j}^n)^2/(h^2) + (\phi_{i,j+1}^n - \phi_{i,j-1}^n)^2/(2h)^2}} \right) \\ & + \frac{\mu}{h^2} \Delta_-^y \cdot \left(\frac{\Delta_+^y \phi_{i,j}^{n+1}}{\sqrt{(\phi_{i+1,j}^n - \phi_{i-1,j}^n)^2/(2h)^2 + (\Delta_+^y \phi_{i,j}^n)^2/(h^2)}} \right) \\ & \left. - \nu - \lambda_1(u_{i,j} - c_1(\phi^n))^2 + \lambda_2(u_{i,j} - c_2(\phi^n))^2 \right] \end{aligned}$$

Principal Steps of the Algorithm

Algorithm 1: The Level-Set Algorithm

Input: Initial level-set function ϕ_0 , $n = 0$

Result: Updated level-set function ϕ

```
1 begin
2   Initialize  $\phi^0$  by  $\phi_0$ ,  $n = 0$ 
3   while the solution is not stationary do
4     Compute  $c_{in}(\phi^n)$  and  $c_{out}(\phi^n)$  based on the current state;
5     Solve the PDE in  $\phi$  from the previous eq., to obtain  $\phi^{n+1}$ ;
6     Check whether the solution is stationary;
7     if not stationary then
8       |    $n = n + 1$ ;
9     end
10  end
```

① Motivation

② The Chan–Vese Model

③ Results

④ Impact on Research

⑤ Concluding Remarks

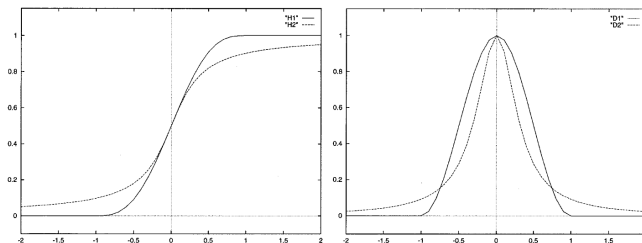
⑥ References

Parameter Selection

- $\lambda_1 = \lambda_2 = 1$, $\nu = 0$, $h = 1$ (the step space), $\Delta t = 0.1$ (the time step).
- $H_{2,\epsilon}$ and $\delta_{2,\epsilon}$ were used with ($\epsilon = h = 1$), in order to automatically detect *interior contours*, and to ensure the computation of a *global minimizer*.
- μ is *experiment-dependent*:
 - Detect as many objects as possible \Rightarrow small μ .
 - Detect only larger objects \Rightarrow large μ .

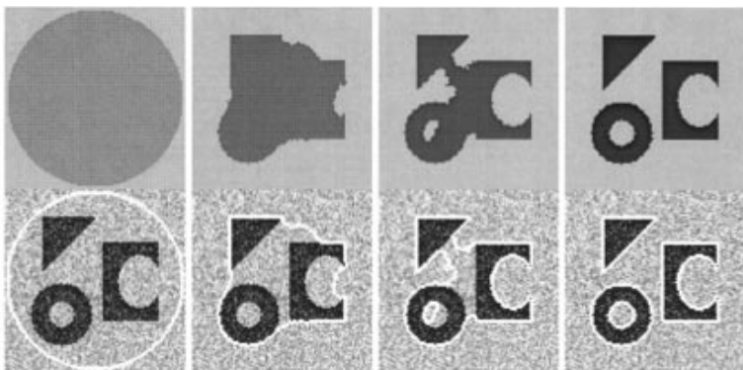
Comparison between $H_{1,\epsilon}$ and $H_{2,\epsilon}$ regularizations

- The energy functional F_ϵ is *non-convex*, allowing therefore many local minima.
- With $H_{1,\epsilon}$ and $\delta_{1,\epsilon} \implies$ local minimizer of the energy.
- With $H_{2,\epsilon}$ and $\delta_{2,\epsilon} \implies$ global minimizer of the energy.



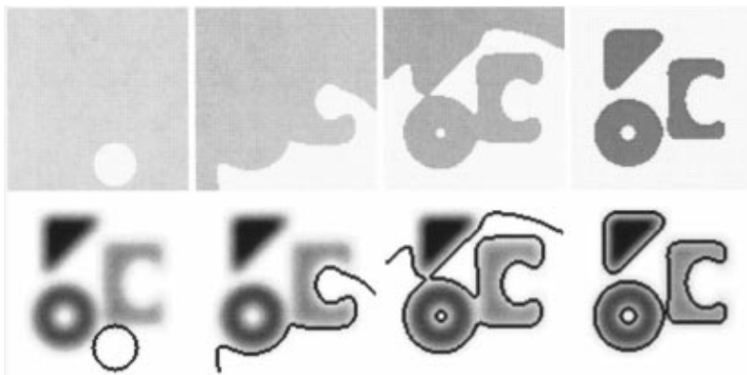
Two different regularizations of the (left) heaviside function H and (right) delta function δ_0 [1]

Results



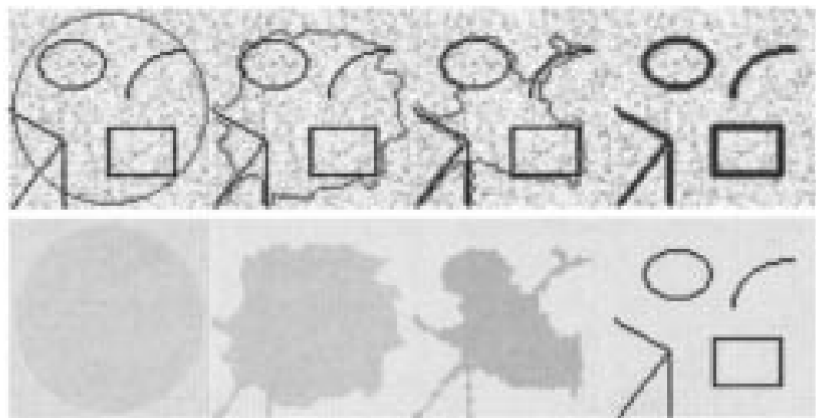
Detection of different objects from a noisy image, with various shapes and with an interior contour. **Left:** u and the contour. **Right:** the piecewise-constant approximation of u . Size = 100×100 , $\phi_0(x, y) = -\sqrt{(x - 50.5)^2 + (y - 50.5)^2} + 48.5$, $\mu = 0.1 \times 255^2$, no reinitialization, cpu = 4.60 s [1].

Results



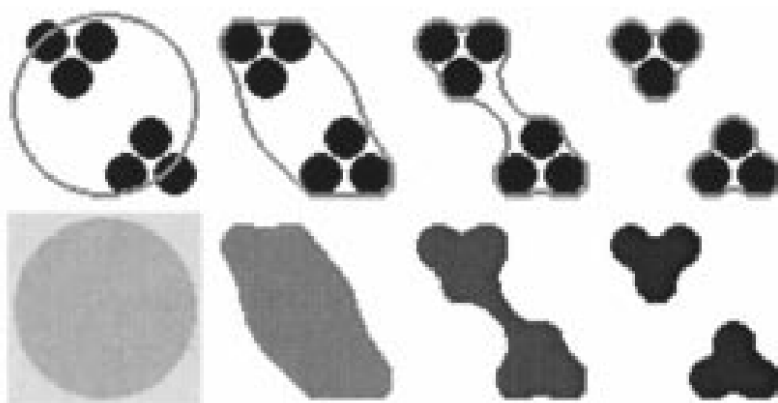
Detection of three blurred objects of distinct intensities. Size = 100×100 , $\phi_0(x, y) = -\sqrt{(x - 15)^2 + (y - 60)^2} + 12$, $\mu = 0.01 \cdot 255^2$, no reinitialization, cpu = 48.67 s [1].

Results



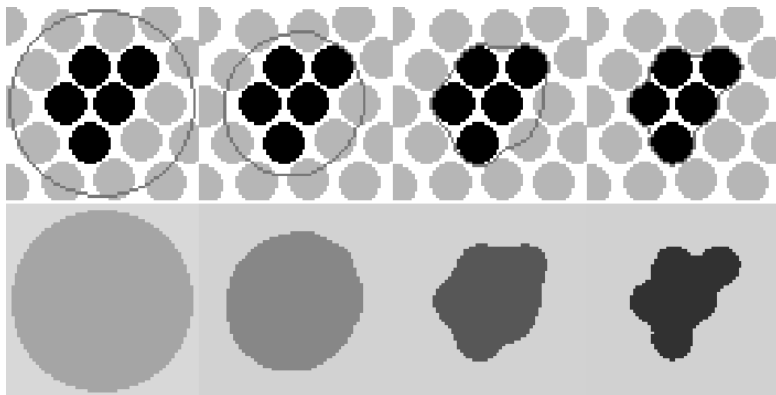
Detection of lines and curves not necessarily closed. Size = 64×64 , $\phi_0(x, y) = -\sqrt{(x - 32.5)^2 + (y - 32.5)^2} + 30$, $\mu = 0.02 \cdot 255^2$, no reinitialization, cpu = 2.88 s [1].

Results



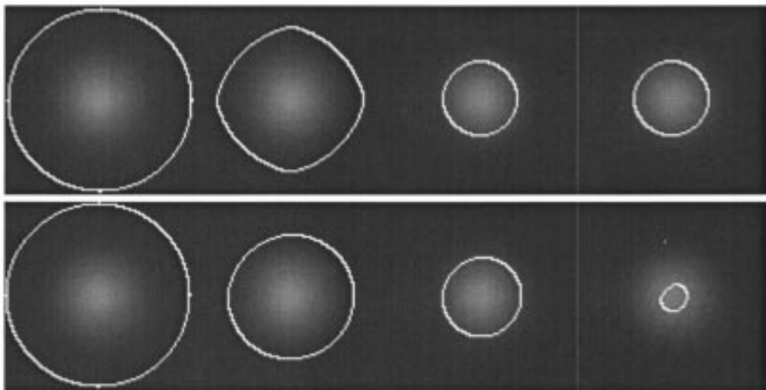
Grouping based on Kanizsa's "proximity rule." Size = 64×64 ,
 $\phi_0(x, y) = -\sqrt{(x - 32.5)^2 + (y - 32.5)^2} + 30$, $\mu = 2 \cdot 255^2$, no reinitialization, cpu = 5.76 s [1].

Results



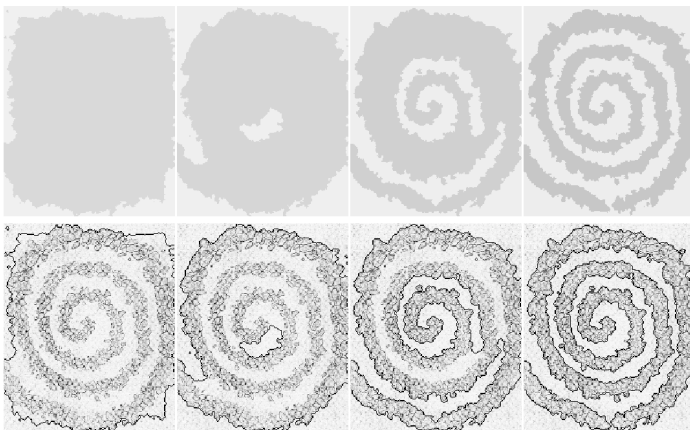
Grouping based on chromatic identity. Size: 64×64 ,
 $\phi_0(x, y) = -\sqrt{(x - 32.5)^2 + (y - 32.5)^2} + 30.5$, $\mu = 2 \cdot 255^2$, no reinitialization, cpu
= 5.76 s. [1].

Results



Object with smooth contour. **Top:** results using the **Chan–Vese model** without edge-function. **Bottom:** results using the classical model (2) with edge-function $g(|\nabla u|)$, by which the curve cannot detect the smooth boundary [1].

Results



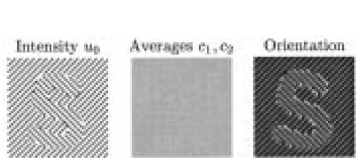
Spiral from an art picture. Size = 234×191 , $\mu = 0.0000033 \cdot 255^2$, five iterations of reinitialization, cpu = 108.85 s [1].

Advantages of the Model

- The ability of detecting smooth boundaries.
- Scale adaptivity (with the parameter μ).
- Automatic change of topology.
- Robustness with respect to noise.
- Flexibility in handling various image types, even without much parameter tuning.

Limitations of the Model

- The **Chan–Vese (2001)** model is a specific case of the Mumford–Shah functional.
- There are objects which cannot be detected using the *average intensity value* only.



Grouping based on orientation identity. The original image u (leftmost) is replaced by the orientation of the normal to the level curves of u . Size: 64×64 , $\mu = 0.025 \cdot 255^2$, $\nu = 0.02 \cdot 255^2$, $\phi_0(x, y) = -\sqrt{(x - 32.5)^2 + (y - 32.5)^2} + 30$, five iterations of reinitialization, cpu = 10.25 s [1].

① Motivation

② The Chan–Vese Model

③ Results

④ Impact on Research

Real-World Applications

Current Approaches

⑤ Concluding Remarks

⑥ References

① Motivation

② The Chan–Vese Model

③ Results

④ Impact on Research

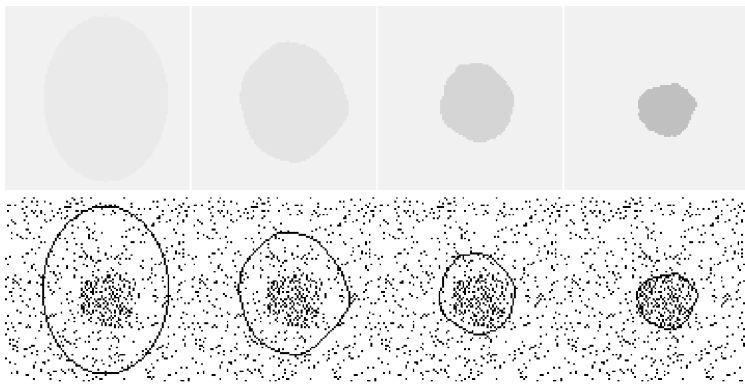
Real-World Applications

Current Approaches

⑤ Concluding Remarks

⑥ References

Segmentation on Satellite Images



Detection of a simulated minefield, with contour without gradient.

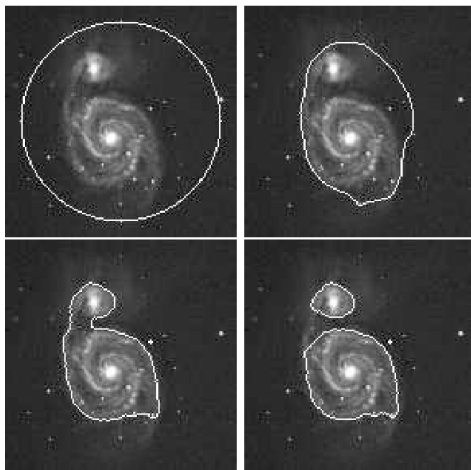
Size = 100×100 , $\phi_0(x, y) = -\sqrt{(x - 50.5)^2 + (y - 50.5)^2} + 47$, $\mu = 0.2 \cdot 255^2$, no reinitialization, cpu = 144.81 s [1].

Segmentation on Satellite Images



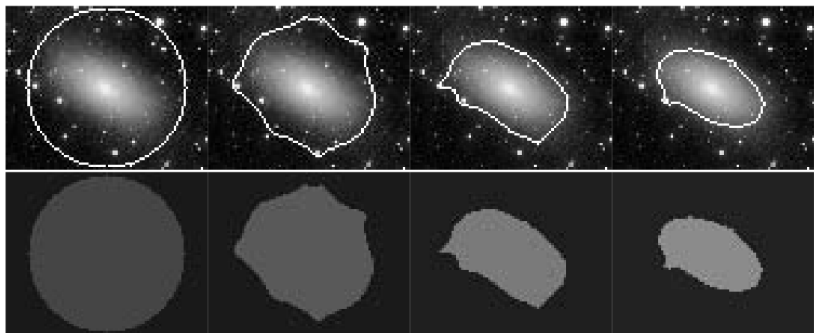
Europe night-lights. Size = 118×113 , $\phi_0(x, y) = -\sqrt{(x - 59.)^2 + (y - 57.)^2} + 55$,
 $\mu = 0.05 \cdot 255^2$, five iterations of reinitialization, cpu = 32.74 s [1].

Segmentation on Satellite Images



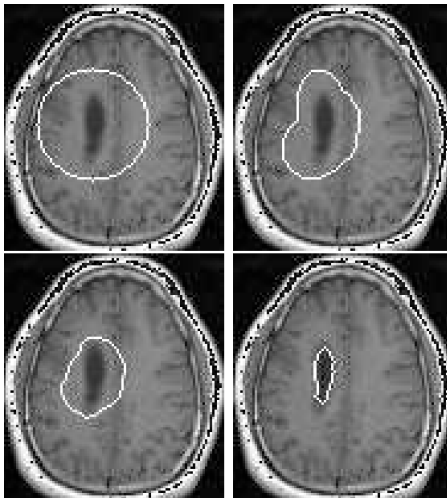
Detection of the contours of a galaxy [1].

Segmentation on Satellite Images



Detection of a galaxy with very smooth boundaries [1].

Segmentation on MRI Images



Detection of a tumor in a MRI image [1].

Implementations

- Available as a segmentation method in *scikit-image* (Python).
- Integrated as a Plugin in MATLAB by Yue Wu.
- Integrated in **Insight Toolkit (ITK)**, an open-source, cross-platform library for image analysis.

The screenshot shows the scikit-image website's 'Examples' page. At the top, there is a navigation bar with the scikit-image logo, 'User guide', and 'Examples' (which is underlined). Below the navigation bar, there is a sidebar with links to 'Normalized Cut', 'Find Regular Segments Using Compact Watershed', 'Thresholding', 'Drawing Region Adjacency Graphs (RAGs)', and 'Chan–Vese Segmentation'. Under 'Chan–Vese Segmentation', there are links to 'Finding local maxima', 'Niblack and Sauvola Thresholding', 'Multi-Otsu Thresholding', and 'Apply maskSLIC vs SLIC'. The main content area displays an example titled 'Chan Vese Active Contours without edges'. It includes a preview image, a brief description, and a link to the source code. Below the preview, there are tabs for 'Übersicht', 'Funktionen', 'Versionenlauf', 'Rezensionen (22)', and 'Diskussionen (0)'. A note at the bottom says 'Implement following papers:' followed by a list of three academic references.

The screenshot shows the ITK website's 'Set Segmentation' page. At the top, there is a navigation bar with the ITK logo, 'Build, Run, Visualize', and 'Contribute'. Below the navigation bar, there is a sidebar with links to 'Geometric Properties of Labeled Region', 'Multiphase Chan and Vese Sparse Field Level Set Segmentation', 'Segment Blood Vessels With Multi-Scale Hessian-Based Measure', 'Singlephase Chan and Vese Dense Field Level Set Segmentation', and 'Singlephase Chan and Vese Sparse Field Level Set Segmentation'. The main content area displays a list of related topics.

Some widely-spread implementations of the **Chan–Vese model** in software.

① Motivation

② The Chan–Vese Model

③ Results

④ Impact on Research

Real-World Applications

Current Approaches

⑤ Concluding Remarks

⑥ References

Derivative Works

| Title | Last Author | Year | Citations |
|---|-------------|------|-----------|
| Level Set Method in Medical Imaging Segmentation | J. Suri | 2019 | 12 |
| Efficient and robust segmentation and correction model for medical images | W. Jia | 2018 | 3 |
| A two-stage image segmentation via global and local region active contours | Yugang Wang | 2016 | 49 |
| Active contours driven by local likelihood image fitting energy for image segmentation | Qiang Chen | 2015 | 94 |
| Robust image segmentation using local robust statistics and correntropy-based K-means clustering | Li Zeng | 2015 | 23 |
| An active contour model and its algorithms with local and global Gaussian distribution fitting energies | Yilun Wang | 2014 | 86 |
| An efficient operator splitting method for local region Chan-Vese model | Jun Liu | 2013 | 2 |

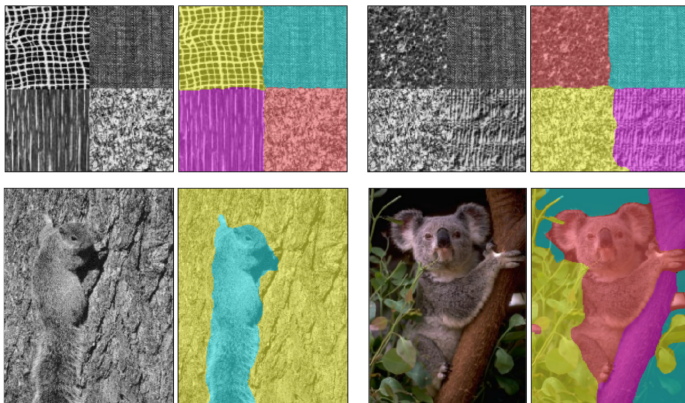
Courtesy of @ConnectedPapers, this table available here.



Extensions of the Chan–Vese Model

- Modifications of the **Chan–Vese model** include [17]:
 - More sophisticated features than the grey value
 - Colour channels, texture features, optic flow fields, ...
 - Additional statistical characterizations of a region
 - Not only mean, but also standard deviation, ...
 - A-priori knowledge, using a statistical characterization of the shapes to be expected
- Can yield excellent segmentation results

Extensions of the Chan–Vese Model



Top: Segmentation of two artificial texture images: In both cases 4 regions were detected.

Bottom left: Segmentation of a squirrel image: 2 regions have been detected.

Bottom right: Segmentation of a koala image (colour): 4 regions have been detected.

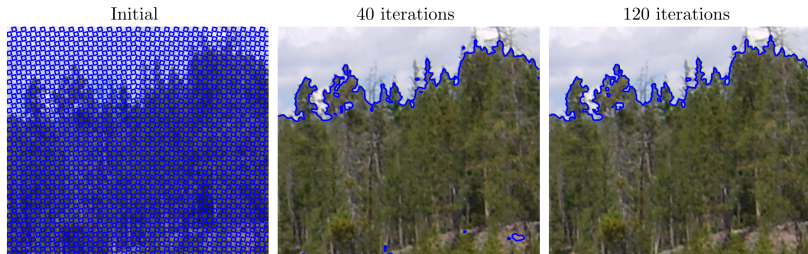
Author: T. Brox (2004) [13].

Extensions of the Chan–Vese Model



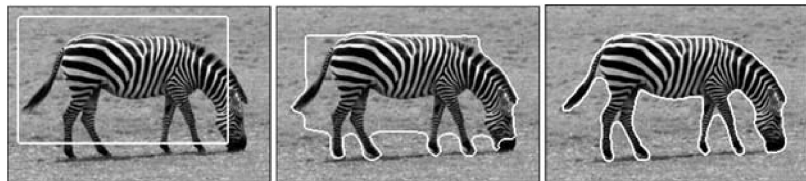
Top: Segmentation of a leopard image (colour): 3 regions have been detected. **Bottom:** Segmentation of a castle image (colour): 3 regions have been detected. Author: T. Brox (2004) [13].

Extensions of the Chan–Vese Model



The **Chan–Sandberg–Vese (2000)** method can be used to segment color images [11]. In this color image, Chan–Sandberg–Vese is applied in the RGB color space to separate the sky from the trees in 120 iterations. Author: P. Getreuer (2012) [15].

Extensions of the Chan–Vese Model



Curve evolution for the segmentation of a zebra image using the nonlinear structure tensor and the smoothed intensity (here, a rectangle is used as initialization but small circles also lead to a similar result). Author: Cremers et al. (2006) [14].

Extensions of the Chan–Vese Model



Sample segmentations using statistical shape priors. From left to right, the shape priors are a single static shape prior (Rousson and Paragios, 2002), uniformly distributed in the PCA subspace (Rousson, 2004), automatically selected from multiple shape instances (Cremers et al., 2006) and dynamical (Cremers, 2006).

① Motivation

② The Chan–Vese Model

③ Results

④ Impact on Research

⑤ Concluding Remarks

⑥ References

Concluding Remarks

- **Chan and Vese (2001)** introduced an active contour model, that did not rely on gradient computation, based on *Mumford–Shah segmentation* and level set methods.
- Robust to noise; no need for initial image smoothing.
- Capable of detecting objects with non-gradient and smooth boundaries.
- Efficiently identifies interior contours with a single initial curve.
- Initial curve placement is flexible; does not need to encircle the target objects.

① Motivation

② The Chan–Vese Model

③ Results

④ Impact on Research

⑤ Concluding Remarks

⑥ References

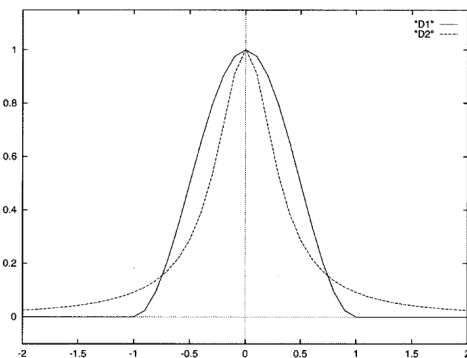
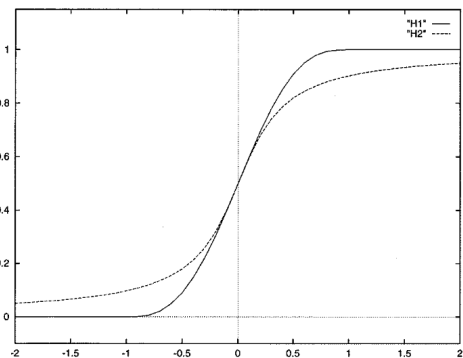
- [1] T.F. Chan and L.A. Vese, *Active contours without edges*, IEEE Transactions on Image Processing, vol. 10, no. 2, pp. 266-277, 2001, doi: 10.1109/83.902291.
- [2] V. Caselles, R. Kimmel, and G. Sapiro, *On geodesic active contours*, International Journal of Computer Vision, vol. 22, pp. 61–79, 1997, doi: 10.1023/A:1007979827043.
- [3] D. Adalsteinsson and J.A. Sethian, *A Fast Level Set Method for Propagating Interfaces*, Journal of Computational Physics, vol. 118, no. 2, pp. 269-277, 1995, doi: 10.1006/jcph.1995.1098.
- [4] S. Kichenassamy, A. Kumar, P. Olver, A. Tannenbaum, and A. Yezzi, *Gradient flows and geometric active contour models*, Proceedings of IEEE International Conference on Computer Vision, pp. 810-815, 1995, doi: 10.1109/ICCV.1995.466855.
- [5] D. Adalsteinsson and J.A. Sethian, *A Fast Level Set Method for Propagating Interfaces*, Journal of Computational Physics, vol. 118, no. 2, pp. 269-277, 1995, doi: 10.1006/jcph.1995.1098.
- [6] R. Malladi, J. A. Sethian, and B. C. Vemuri, *A topology independent shape modeling scheme*, in Proc. SPIE Conf. Geometric Methods Computer Vision II, vol. 2031, San Diego, CA, 1993, pp. 246–258.

- [7] M. Kass, A. Witkin, and D. Terzopoulos, *Snakes: Active contour models*, Int. J. Comput. Vis., vol. 1, pp. 321–331, 1988.
- [8] S. Osher and J.A. Sethian, *Fronts propagating with curvature-dependent speed: Algorithms based on Hamilton-Jacobi formulations*, Journal of Computational Physics, vol. 79, no. 1, pp. 12-49, 1988, doi: 10.1016/0021-9991(88)90002-2.
- [9] D. Mumford and J. Shah, *Boundary detection by minimizing functionals*, IEEE CVPR, vol. 17, pp. 22-26, 1985.
- [10] H.-K. Zhao, T. Chan, B. Merriman, and S. Osher, *A variational level set approach to multiphase motion*, in J. Comput. Phys., vol. 127, 1996, pp. 179–195.
- [11] T. F. Chan, B. Sandberg, and L. A. Vese, *Active Contours Without Edges for Vector-Valued Images*, Journal of Visual Communication and Image Representation, vol. 11, pp. 130–141, 2000. Available: <http://dx.doi.org/10.1006/jvci.1999.0442>
- [12] M. Rousson and N. Paragios, *Shape Priors for Level Set Representations*, in Computer Vision — ECCV 2002, A. Heyden, G. Sparr, M. Nielsen, and P. Johansen, Eds. Berlin, Heidelberg: Springer Berlin Heidelberg, 2002, pp. 78–92.

- [13] T. Brox and J. Weickert, *Level Set Based Image Segmentation with Multiple Regions*, in Pattern Recognition, C. E. Rasmussen, H. H. Bülfhoff, B. Schölkopf, and M. A. Giese, Eds. Berlin, Heidelberg: Springer Berlin Heidelberg, 2004, pp. 415–423, doi: 10.1007/978-3-540-28649-3_51.
- [14] D. Cremers, *Dynamical statistical shape priors for level set-based tracking*, IEEE Transactions on Pattern Analysis and Machine Intelligence, vol. 28, no. 8, pp. 1262-1273, 2006, doi: 10.1109/TPAMI.2006.161.
- [15] P. Getreuer, *Chan-Vese Segmentation*, Image Processing On Line, vol. 2, pp. 214–224, 2012. Available: <https://doi.org/10.5201/ipol.2012.g-cv>
- [16] Martínez, C. (2021). *Aplicación de la visión por computadora en el análisis de microestructuras y la obtención de relaciones estructura - propiedad*. Universidad de los Andes. Retrieved from <http://hdl.handle.net/1992/51616> ([Online; accessed 25.06.2024]).
- [17] P. Pascal, *Differential equations in computer vision, Lecture 25: Self-snakes and Active Contours*, Universität des Saarlandes, 2023.
- [18] Wikipedia contributors, *Lipschitz continuity — Wikipedia, The Free Encyclopedia*, Retrieved from https://en.wikipedia.org/wiki/Lipschitz_continuity ([Online; accessed 23.06.2024]).

- [19] Wikipedia contributors, *Heaviside step function — Wikipedia, The Free Encyclopedia*, Retrieved from https://en.wikipedia.org/wiki/Heaviside_step_function ([Online; accessed 23.06.2024]).
- [20] Wikipedia contributors, *Dirac delta function — Wikipedia, The Free Encyclopedia*, Retrieved from https://en.wikipedia.org/wiki/Dirac_delta_function ([Online; accessed 23.06.2024]).
- [21] Viso.ai, *Image Segmentation with Deep Learning (Guide)*, Retrieved from <https://viso.ai/deep-learning/image-segmentation-using-deep-learning/> ([Online; accessed 25.06.2024]).
- [22] N. Alarcon, *Automatically Segmenting Brain Tumors with AI*, NVIDIA Developer Blog, Retrieved from <https://developer.nvidia.com/blog/automatically-segmenting-brain-tumors-with-ai/> ([Online; accessed 25.06.2024]).
- [23] J. Eglinger, *Texture Segmentation*, image.sc Forum, Retrieved from <https://forum.image.sc/t/texture-segmentation/69785> ([Online; accessed 25.06.2024]).

Appendix



Two different regularizations of the (left) heaviside function H and (right) delta function δ_0 [1].